Available online at www.sciencedirect.com
ScienceDirect
Journal of the Mechanics and Physics of Solids
55 (2007) 1001–1015

JOURNAL OF THE MECHANICS AND PHYSICS OF SOLIDS

www.elsevier.com/locate/jmps

Bio-inspired mechanics of reversible adhesion: Orientation-dependent adhesion strength for non-slipping adhesive contact with transversely isotropic elastic materials

Shaohua Chen[a], Huajian Gao[b,*]

[a]*LNM, Institute of Mechanics, Chinese Academy of Sciences, Beijing 100080, China*
[b]*Division of Engineering, Brown University, Providence, RI 02912, USA*

Received 26 July 2006; received in revised form 25 October 2006; accepted 28 October 2006

Abstract

Geckos and many insects have evolved elastically anisotropic adhesive tissues with hierarchical structures that allow these animals not only to adhere robustly to rough surfaces but also to detach easily upon movement. In order to improve our understanding of the role of elastic anisotropy in reversible adhesion, here we extend the classical JKR model of adhesive contact mechanics to anisotropic materials. In particular, we consider the plane strain problem of a rigid cylinder in non-slipping adhesive contact with a transversely isotropic elastic half space with the axis of symmetry oriented at an angle inclined to the surface. The cylinder is then subjected to an arbitrarily oriented pulling force. The critical force and contact width at pull-off are calculated as a function of the pulling angle. The analysis shows that elastic anisotropy leads to an orientation-dependent adhesion strength which can vary strongly with the direction of pulling. This study may suggest possible mechanisms by which reversible adhesion devices can be designed for engineering applications.

Keywords: Adhesion and adhesives; Releasable adhesion; Anisotropic material; Biological material; Contact mechanics

*Corresponding author. Tel.: +1 401 863 2626.
E-mail address: Huajian_Gao@Brown.edu (H. Gao).

0022-5096/$ - see front matter © 2006 Elsevier Ltd. All rights reserved.
doi:10.1016/j.jmps.2006.10.008

1. Introduction

Adhesion systems in biology, including those of gecko and many insects, have attracted significant attention in recent years (e.g., Hiller, 1968; Autumn et al., 2000, 2002; Autumn and Peattie, 2002; Russell, 2002; Arzt et al., 2002, 2003; Gao and Yao, 2004; Glassmaker et al., 2004; Hui et al., 2004; Gao et al., 2005; Spolenak et al., 2005; Huber et al., 2005; Yao and Gao, 2006). On one hand, the adhesion mechanisms in biology must be robust enough to function on rough surfaces. On the other hand, bio-adhesion must be easily releasable upon animal movement. While structural hierarchy seems to play a critical role in robust adhesion, elastic anisotropy appears to play a key role in the reversibility of biological adhesion (Autumn et al., 2000; Gorb and Scherge, 2000; Niederegger et al., 2002; Yao and Gao, 2006). For example, the tissue on gecko's feet is made of hundreds of thousands of keratinous hairs called setae, the tips of which further contain hundreds of smaller hairs called spatulae with typical diameters on the order of a few hundred nanometers. This hairy microstructure results in a hierarchical and strongly anisotropic tissue which leads to robust and reversible adhesion.

Recent developments in experimental techniques to measure adhesive forces at the level of individual setae (Autumn et al., 2000, 2002) and spatulae (Kesel et al., 2003; Langer et al., 2004; Huber et al., 2005) are calling for more systematic theoretical and experimental studies of adhesion mechanisms in biology. A systematic study of biological adhesion mechanisms should be of interest not only to the understanding of biological systems but also to the development of novel adhesive materials or devices for engineering applications.

Reversible adhesion has been studied at the level of a single seta of gecko (Autumn et al., 2000; Gao et al., 2005). Autumn et al. (2000) reported that a single seta exhibits strong adhesive force at a pulling angle around 30°. Gao et al. (2005) numerically simulated the pull-off force of a single seta and found that the asymmetrical alignment of seta allows the pull-off force to vary strongly with the direction of pulling. Such anisotropic adhesion behavior of a discrete structure is in fact quite similar to that of an elastic tape on substrate (Kendall, 1975; Spolenak et al., 2005; Huber et al., 2005). On the other hand, at the tissue level, there has been relatively little study on how reversible adhesion can be achieved on larger scales (Yao and Gao, 2006). An interesting observation is that, while geckos and some insects have adopted hairy tissues for robust and reversible adhesion, some other insects seem to have achieved this via smooth tissues. For example, the attachment pad of cicada exhibits a smooth outer membranous layer covering an anisotropic microstructure made of highly elongated foams (Scherge and Gorb, 2001). The attachment pad of grasshopper shows a smooth membrane covering arrays of cross-linked rod-like fibers that are branches of thicker principal rods located deeper in the cuticle and oriented at some angle to the cuticle surface (Slifer, 1950; Kendall, 1970). These biological adhesion systems show two kinds of microstructure designs, i.e., the hairy and the smooth attachment pads. Through a comparative study of various biological attachment pads in more than 300 species of insects, Gorb and Beutel (2001) and Beutel and Gorb (2001) pointed out that the main similarity of both designs is that the structured pad surfaces or particular properties of the pad materials guarantee a maximum real contact area with diverse substrates. Yao and Gao (2006) argued that the most important feature of biological adhesion systems that leads to reversible adhesion is the strong elastic anisotropy in the overall property of the tissues. They used an interfacial crack model to show that adhesion between two

three-dimensional anisotropic elastic solids exhibit orientation-dependent failure strength. In other words, the binding strength of two anisotropic elastic continuum, even without a microstructure, would vary strongly with the direction of pulling.

The present paper is aimed to develop a model of reversible adhesion within the framework of adhesive contact mechanics which has so far been largely limited to isotropic materials (Johnson et al., 1971; Derjaguin et al., 1975; Roberts and Thomas, 1975; Muller et al., 1980; Greenwood and Johnson, 1981; Barquins, 1988; Maugis, 1992; Carpick et al., 1996; Chaudhury et al., 1996; Baney and Hui, 1997; Greenwood, 1997; Johnson and Greenwood, 1997; Barthel, 1998; Greenwood and Johnson, 1998; Robbe-Valloire and Barquins, 1998; Kim et al., 1998; Morrow et al., 2003; Schwarz, 2003; Chen and Gao, 2006a, b, c ; Chen and Wang, 2006). Our model provides a connection between the interfacial fracture model for reversible adhesion by Yao and Gao (2006) and the contact mechanics models. In particular, we consider the plane strain problem of a rigid cylinder in contact with a transversely isotropic elastic solid subjected to an arbitrarily oriented detachment force in the plane of the analysis. The contact region is assumed to be non-slipping such that both tangential and normal tractions are transmitted across the contact interface.

The plan of the paper is as follows. First, the Barnett–Lothe tensors for transversely isotropic materials are introduced to facilitate the subsequent analysis. Next, the anisotropic contact model is set up and the Griffith energy balance between elastic and surface energies is used to determine the relationship between the applied pulling force and the size of the contact region. Of special interest is the critical force at pull-off as a function of the pulling angle and the orientation of the symmetry axis of the material.

2. Barnett–Lothe tensors for transversely isotropic materials

Transversely isotropic materials are a special class of anisotropic materials that are isotropic in a plane (taken to be the x_0–z_0 plane) and anisotropic out of this plane. The vector normal to the isotropic plane, taken to be the y_0-axis, forms a symmetry axis of the material. Such materials are described by five independent elastic constants: Young's modulus and Poisson ratio in the isotropic plane (E_1 and v_1); Young's modulus, Poisson ratio and shear modulus associated with the out-of-plane direction (E_2, v_2 and G_{12}).

In subsequent analysis we will make use of the Barnett–Lothe tensors (e.g., Ting, 1996) whose expressions for orthotropic materials have been given by Dongye and Ting (1989) and Hwu (1993). For transversely isotropic materials, they are defined as

$$\boldsymbol{S} = \begin{bmatrix} 0 & s_{12} \\ s_{21} & 0 \end{bmatrix}, \quad \boldsymbol{L} = \begin{bmatrix} L_{11} & 0 \\ 0 & L_{22} \end{bmatrix}, \tag{1}$$

where

$$s_{12} = -\alpha_2\gamma_1\chi_1, \quad s_{21} = \alpha_1\gamma_2\chi_1, \tag{2}$$

$$L_{11} = \alpha_1\gamma_1 E_1, \quad L_{22} = \alpha_2\gamma_2 E_2, \tag{3}$$

$$\begin{cases} \gamma_1 = \left(E_1/G_{12} + 2\chi_1\sqrt{E_1/E_2}\right)^{-1/2}, & \gamma_2 = \left(E_2/G_{12} + 2\chi_1\sqrt{E_2/E_1}\right)^{-1/2}, \\ \alpha_1 = (1-v_1^2)^{-1/2}, & \alpha_2 = \left(1 - \dfrac{v_2^2 E_1}{E_2}\right)^{-1/2}, \\ \chi_1 = \sqrt{(1-v_1^2)\left(1 - \dfrac{v_2^2 E_1}{E_2}\right)} - (1+v_1)v_2\sqrt{\dfrac{E_1}{E_2}} \end{cases} \tag{4}$$

and

$$L_{22}/L_{11} = \frac{\alpha_2}{\alpha_1}\sqrt{\frac{E_2}{E_1}}. \tag{5}$$

3. The model

To understand the mechanism of reversible adhesion in anisotropic solids, we consider the plane strain contact model described in Fig. 1. A rigid cylinder of radius R is shown to be in contact with a transversely isotropic elastic half space whose symmetry axis is inclined at an angle θ. An external force F is applied to pull the cylinder in a direction ϕ. The width of the contact region is $2a$. A Cartesian coordinate system (x, y) is attached to

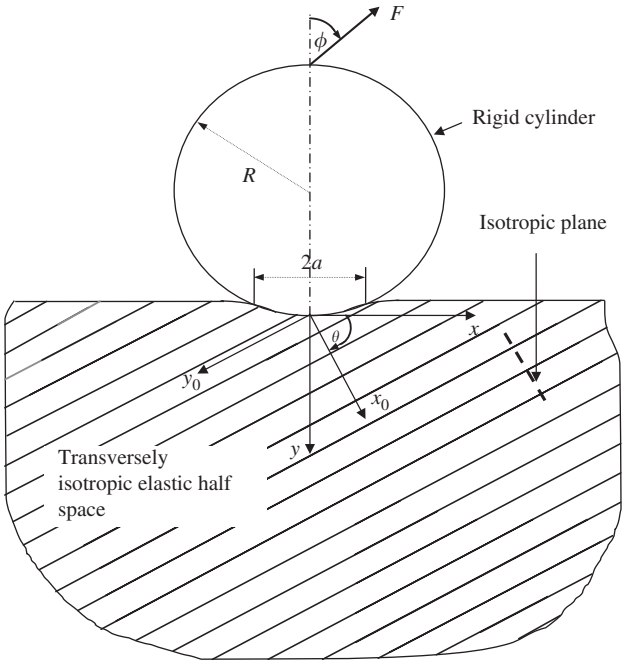

Fig. 1. A rigid cylinder of radius R contacting a transversely isotropic elastic half space with the axis of material symmetry inclined at an angle θ with respect to the normal of the surface. A Cartesian coordinate system (x, y) is fixed at the center of the contact region of width $2a$. An external pulling force F is applied on the cylinder at an angle ϕ from the y-axis.

the center of the contact region, with the y-axis pointing into the elastic half space. The contact region is assumed to be perfectly bonded, with $P(x)$ and $Q(x)$ denoting, respectively, the normal and tangential tractions along the contact interface. The pulling force is assumed to be properly aligned such that there is no net bending moment on the contact region. The edges of the contact region resemble two opposing interfacial cracks under plane strain deformation. As in almost all contact mechanics theories (Johnson, 1985), the contact width is assumed to be small compared to the radius of the cylinder.

Under the above assumptions, the continuity across the interface requires the tangential and normal displacements along the surface of the elastic half space to be equal to

$$\bar{u}_x = 0, \quad |x| \leqslant a, \tag{6}$$

$$\bar{u}_y = \delta - \frac{x^2}{2R}, \quad |x| \leqslant a, \tag{7}$$

where δ is a constant and R the radius of the cylinder (see Johnson, 1985).

Differentiating Eqs. (6) and (7) with respect to x gives

$$\begin{cases} \dfrac{\partial \bar{u}_x}{\partial x} = 0, \\ \dfrac{\partial \bar{u}_y}{\partial x} = -\dfrac{x}{R}. \end{cases} \tag{8}$$

These surface displacements can be related to the surface tractions $Q(x)$ and $P(x)$ via Green's functions of a tilted transversely isotropic elastic half space (e.g., Ting, 1996). When this is done, Eq. (8) becomes

$$\frac{1}{\pi}\int_{-a}^{a} \frac{\boldsymbol{D}}{s-x}\boldsymbol{f}(s)\,\mathrm{d}s + \boldsymbol{W}\boldsymbol{f}(x) = \boldsymbol{C}, \tag{9}$$

where the coefficient matrices can be expressed in terms of the Barnett–Lothe tensors as

$$\boldsymbol{D} = \boldsymbol{\Omega}\boldsymbol{D}_0\boldsymbol{\Omega}^{\mathrm{T}}, \quad \boldsymbol{D}_0 = \boldsymbol{L}^{-1}, \tag{10}$$

$$\boldsymbol{W} = -\boldsymbol{\Omega}\boldsymbol{W}_0\boldsymbol{\Omega}^{\mathrm{T}} = -\boldsymbol{W}_0, \quad \boldsymbol{W}_0 = \boldsymbol{S}\boldsymbol{L}^{-1} = \begin{bmatrix} 0 & W_{12} \\ W_{21} & 0 \end{bmatrix}, \tag{11}$$

$$\boldsymbol{C} = \begin{bmatrix} 0 \\ \frac{-x}{R} \end{bmatrix}, \quad \boldsymbol{f}(x) = \begin{pmatrix} Q(x) \\ P(x) \end{pmatrix}, \tag{12}$$

$$\boldsymbol{\Omega} = \begin{bmatrix} \cos\theta & -\sin\theta \\ \sin\theta & \cos\theta \end{bmatrix}. \tag{13}$$

Superscript "T" denotes matrix transposition, subscript "0" stands for matrices with material symmetric axis coincident with the normal of the contact interface, i.e., $\theta = 0$.

We note the following properties of these matrices:

$$\boldsymbol{\Omega}^{-1} = \boldsymbol{\Omega}^{\mathrm{T}}, \quad \boldsymbol{D}^{-1} = \boldsymbol{\Omega}\boldsymbol{L}\boldsymbol{\Omega}^{\mathrm{T}}, \quad W_{12} = \frac{s_{12}}{L_{22}}, \quad W_{21} = \frac{s_{21}}{L_{11}}, \tag{14}$$

$$\boldsymbol{D}_0 = \begin{bmatrix} d_{11} & 0 \\ 0 & d_{22} \end{bmatrix} = \boldsymbol{L}^{-1} = \begin{bmatrix} \frac{1}{L_{11}} & 0 \\ 0 & \frac{1}{L_{22}} \end{bmatrix}, \quad W_{21} = -W_{12}. \tag{15}$$

The components of the matrix

$$\boldsymbol{D}^{-1} = \begin{bmatrix} D_{11}^{*-1} & D_{12}^{*-1} \\ D_{21}^{*-1} & D_{22}^{*-1} \end{bmatrix} \tag{16}$$

are explicitly written as

$$D_{11}^{*} = \frac{1}{L_{11}\cos^2\theta + L_{22}\sin^2\theta}, \quad D_{22}^{*} = \frac{1}{L_{11}\sin^2\theta + L_{22}\cos^2\theta}, \tag{17}$$

$$D_{12}^{*} = D_{21}^{*} = \frac{1}{(L_{11} - L_{22})\cos\theta\,\sin\theta}. \tag{18}$$

Eq. (9) can be rewritten in the form

$$\frac{1}{\pi}\int_{-a}^{a} \frac{\boldsymbol{I}}{s-x}\boldsymbol{f}(s)\,\mathrm{d}s + \boldsymbol{D}^{-1}\boldsymbol{W}\boldsymbol{f}(x) = \boldsymbol{G}, \tag{19}$$

where

$$\boldsymbol{I} = \begin{bmatrix} 1 & 0 \\ 0 & 1 \end{bmatrix}, \quad \boldsymbol{G} = \boldsymbol{D}^{-1}\boldsymbol{C}. \tag{20}$$

The solution to Eq. (19) with boundary conditions

$$\int_{-a}^{a} P(x)\,\mathrm{d}x = -F\cos\phi, \quad \int_{-a}^{a} Q(x)\,\mathrm{d}x = F\sin\phi \tag{21}$$

can be obtained following a similar procedure used in Chen and Gao (2006a). The calculations are quite lengthy but the methodology of solving such integral equations is standard. We skip all the details and present only the final solution. The interfacial tractions in the contact region have the solution

$$\begin{Bmatrix} Q(x) \\ P(x) \end{Bmatrix} = \begin{Bmatrix} 2\,\mathrm{Re}\{T_1^{+} - T_1^{-}\} \\ -2D_{11}^{*}\,\mathrm{Im}\{\overline{d}_1(T_1^{+} - T_1^{-})\} \end{Bmatrix}, \tag{22}$$

where

$$T_1^{+} = \frac{xd_1}{4R(1-\eta)} + \frac{(a+x)^{-\bar{r}}(a-x)^{-r}d_1}{4\pi\mathrm{i}R(1-\eta)}\int_{-a}^{a}\frac{t(a+t)^{\bar{r}}(a-t)^{r}}{t-x}\,\mathrm{d}t + \kappa_1(a+x)^{-\bar{r}}(a-x)^{-r}\mathrm{e}^{-\pi r\mathrm{i}}, \tag{23}$$

$$T_1^{-} = \frac{xd_1}{4R(1+\eta)} + \frac{(a+x)^{-\bar{r}}(a-x)^{-r}d_1\,\mathrm{e}^{2\pi r\mathrm{i}}}{4\pi\mathrm{i}R(1-\eta)}\int_{-a}^{a}\frac{t(a+t)^{\bar{r}}(a-t)^{r}}{t-x}\,\mathrm{d}t + \kappa_1(a+x)^{-\bar{r}}(a-x)^{-r}\mathrm{e}^{\pi r\mathrm{i}}. \tag{24}$$

The order of stress singularity r is given by

$$r = \tfrac{1}{2} + \mathrm{i}\varepsilon, \quad \varepsilon = \frac{1}{2\pi}\ln\frac{1+\eta}{1-\eta}, \tag{25}$$

where ε is called the oscillation index and η a bimaterial constant (analogous to Dundurs (1969) parameters β for isotropic materials),

$$\eta = \left| W_{21}\sqrt{\frac{1}{D_{11}^* D_{22}^*} - \frac{1}{D_{12}^{*2}}} \right|. \tag{26}$$

The constants d_1 and κ_1 in Eqs. (22)–(24) are

$$d_1 = \frac{\mathrm{i}}{D_{12}^*} + \sqrt{\frac{1}{D_{11}^* D_{22}^*} - \frac{1}{D_{12}^{*2}}} \tag{27}$$

$$\kappa_1 = \frac{\sqrt{1-\eta^2}}{4\int_{-a}^{a}(a+x)^{-\bar{r}}(a-x)^{-r}\,\mathrm{d}x}\left[\frac{-F(D_{12}^*\cos\phi + D_{11}^*\sin\phi)}{D_{11}^* D_{12}^*\sqrt{1/D_{11}^* D_{22}^* - 1/D_{12}^{*2}}} + \mathrm{i}F\sin\phi\right]. \tag{28}$$

The stress intensity factor for an interfacial crack between two dissimilar anisotropic solids can be defined as (Wu, 1990; Hwu, 1993; Ting, 1996)

$$\boldsymbol{K} = \lim_{x\to a}\sqrt{2\pi(a-x)}\boldsymbol{\Lambda}\left\langle\left\langle\left(\frac{a-x}{l}\right)^{\mathrm{i}\varepsilon_\alpha}\right\rangle\right\rangle\boldsymbol{\Lambda}^{-1}\boldsymbol{f} = \begin{Bmatrix} K_{\mathrm{II}} \\ -K_{\mathrm{I}} \end{Bmatrix}, \quad \alpha = 1,2, \tag{29}$$

where

$$\boldsymbol{\Lambda} = \boldsymbol{\Omega}\boldsymbol{\Lambda}_0, \quad \boldsymbol{\Lambda}_0 = \begin{bmatrix} \dfrac{-\mathrm{i}}{\sqrt{2d_{11}}} & \dfrac{\mathrm{i}}{\sqrt{2d_{11}}} \\ \dfrac{1}{\sqrt{2d_{22}}} & \dfrac{1}{\sqrt{2d_{22}}} \end{bmatrix}, \tag{30}$$

$$\varepsilon_1 = \varepsilon, \quad \varepsilon_2 = -\varepsilon. \tag{31}$$

The angular bracket $\langle\langle\ \rangle\rangle$ stands for a diagonal matrix, i.e., $\langle\langle\rho_\alpha\rangle\rangle = \mathrm{diag}[\rho_1\ \rho_2]$. Constants d_{11} and d_{22} have been defined in Eq. (15), $\boldsymbol{\Omega}$ in Eq. (13), ε in Eq. (25) and $\boldsymbol{f}$ in Eq. (12).

Using Eqs. (30) and (31), the stress intensity factors in Eq. (29) can be expressed explicitly as

$$\begin{Bmatrix} K_{\mathrm{II}} \\ -K_{\mathrm{I}} \end{Bmatrix} = \lim_{x\to a}\sqrt{2\pi}(a-x)^{1/2}\begin{bmatrix} m_{11} & m_{12} \\ m_{21} & m_{22} \end{bmatrix}\cdot\begin{Bmatrix} Q(x) \\ P(x) \end{Bmatrix}, \tag{32}$$

where

$$m_{11} = \mathrm{Re}\left\{\left[1 + \left(\sqrt{\frac{d_{22}}{d_{11}}} - \sqrt{\frac{d_{11}}{d_{22}}}\right)\mathrm{i}\sin\theta\cos\theta\right]\left(\frac{a-x}{l}\right)^{\mathrm{i}\varepsilon}\right\}, \tag{33}$$

$$m_{12} = \left(\frac{\cos^2\theta\sqrt{d_{22}}}{\sqrt{d_{11}}} + \frac{\sin^2\theta\sqrt{d_{11}}}{\sqrt{d_{22}}}\right)\mathrm{Im}\left\{\left(\frac{a-x}{l}\right)^{\mathrm{i}\varepsilon}\right\}, \tag{34}$$

$$m_{21} = -\left(\frac{\cos^2\theta\sqrt{d_{11}}}{\sqrt{d_{22}}} + \frac{\sin^2\theta\sqrt{d_{22}}}{\sqrt{d_{11}}}\right)\mathrm{Im}\left\{\left(\frac{a-x}{l}\right)^{\mathrm{i}\varepsilon}\right\}, \tag{35}$$

$$m_{22} = \mathrm{Re}\left\{\left[1 - \left(\sqrt{\frac{d_{22}}{d_{11}}} - \sqrt{\frac{d_{11}}{d_{22}}}\right)\mathrm{i}\sin\theta\cos\theta\right]\left(\frac{a-x}{l}\right)^{\mathrm{i}\varepsilon}\right\}. \tag{36}$$

Using the following two identities:

$$1+\left(\sqrt{\frac{d_{22}}{d_{11}}}-\sqrt{\frac{d_{11}}{d_{22}}}\right)\mathrm{i}\,\sin\theta\cos\theta = \left(\frac{\cos^2\theta\sqrt{d_{22}}}{\sqrt{d_{11}}}+\frac{\sin^2\theta\sqrt{d_{11}}}{\sqrt{d_{22}}}\right)\left(\frac{D_{11}^{*}i}{D_{12}^{*}}+\sqrt{\frac{D_{11}^{*}}{D_{22}^{*}}-\frac{D_{11}^{*2}}{D_{12}^{*2}}}\right), \tag{37}$$

$$1-\left(\sqrt{\frac{d_{22}}{d_{11}}}-\sqrt{\frac{d_{11}}{d_{22}}}\right)\mathrm{i}\,\sin\theta\cos\theta = \left(\frac{\cos^2\theta\sqrt{d_{11}}}{\sqrt{d_{22}}}+\frac{\sin^2\theta\sqrt{d_{22}}}{\sqrt{d_{11}}}\right)\left(\frac{-D_{22}^{*}i}{D_{12}^{*}}+\sqrt{\frac{D_{22}^{*}}{D_{11}^{*}}-\frac{D_{22}^{*2}}{D_{12}^{*2}}}\right), \tag{38}$$

the stress intensity factors can be written in the form,

$$K_{\mathrm{I}}=\frac{a^{3/2}}{\sqrt{\pi}R(1-\eta^2)}[B\,\mathrm{Re}\{I_1\}-C\,\mathrm{Im}\{I_1\}]-\frac{\sqrt{\pi}BF}{\sqrt{a}}[B\,\mathrm{Im}\{I_2\}+C\,\mathrm{Re}\{I_2\}], \tag{39}$$

$$K_{\mathrm{II}}=\frac{a^{3/2}A}{\sqrt{\pi}R(1-\eta^2)}\,\mathrm{Im}\{I_1\}+\frac{\sqrt{\pi}AF}{\sqrt{a}}\,\mathrm{Re}\{I_2\}, \tag{40}$$

where

$$I_1=d_1\left(\frac{2a}{l}\right)^{\mathrm{i}\varepsilon}\int_{-1}^{1}\frac{t(1+t)^{\bar{r}}(1-t)^{r}}{t-1}\,\mathrm{d}t, \tag{41}$$

$$I_2=\frac{g(\phi)}{\int_{-1}^{1}(1+\xi)^{-\bar{r}}(1-\xi)^{-r}\,\mathrm{d}\xi}\left(\frac{2a}{l}\right)^{\mathrm{i}\varepsilon}, \tag{42}$$

and

$$A=\frac{D_{22}^{*}}{D_{12}^{*}}\sqrt{\frac{D_{12}^{*2}}{D_{11}^{*}D_{22}^{*}}-1}\left(\frac{\sqrt{d_{11}}}{\sqrt{d_{22}}}\cos^2\theta+\frac{\sqrt{d_{22}}}{\sqrt{d_{11}}}\sin^2\theta\right), \tag{43}$$

$$B=\left(\frac{D_{11}^{*}D_{22}^{*}}{D_{12}^{*2}}-1\right)\left(\frac{\sqrt{d_{11}}}{\sqrt{d_{22}}}\cos^2\theta+\frac{\sqrt{d_{22}}}{\sqrt{d_{11}}}\sin^2\theta\right), \tag{44}$$

$$C=\frac{D_{11}^{*}D_{22}^{*}}{D_{12}^{*2}}\sqrt{\frac{D_{12}^{*2}}{D_{11}^{*}D_{22}^{*}}-1}\left(\frac{\sqrt{d_{11}}}{\sqrt{d_{22}}}\cos^2\theta+\frac{\sqrt{d_{22}}}{\sqrt{d_{11}}}\sin^2\theta\right), \tag{45}$$

$$g(\phi)=\sin\phi+\frac{\mathrm{i}(D_{12}^{*}\cos\phi+D_{11}^{*}\sin\phi)}{D_{11}^{*}D_{12}^{*}\sqrt{\dfrac{1}{D_{11}^{*}D_{22}^{*}}-\dfrac{1}{D_{12}^{*2}}}}. \tag{46}$$

The energy release rate is (Ting, 1996; Wu, 1990)

$$G=\tfrac{1}{4}\boldsymbol{K}^{\mathrm{T}}\boldsymbol{E}K, \tag{47}$$

where

$$\boldsymbol{E} = \boldsymbol{D} + \boldsymbol{W}\boldsymbol{D}^{-1}\boldsymbol{W} = \frac{1}{\cosh^2 \pi\varepsilon}\boldsymbol{D}, \tag{48}$$

Substituting Eqs. (14) and (15) into (48) then into (47) yields the energy release rate

$$G = \frac{1}{4}\frac{D_{11}^* D_{22}^* D_{12}^{*2}}{D_{12}^{*2} - D_{11}^* D_{22}^*}\frac{1}{\cosh^2 \pi\varepsilon}\left(\frac{K_{\mathrm{I}}^2}{D_{11}^*} + \frac{K_{\mathrm{II}}^2}{D_{22}^*} + \frac{2K_{\mathrm{I}}K_{\mathrm{II}}}{D_{12}^*}\right). \tag{49}$$

Substituting Eqs. (39) and (40) into Eq. (49) leads to

$$\begin{aligned}&\frac{K_{\mathrm{I}}^2}{D_{11}^*} + \frac{K_{\mathrm{II}}^2}{D_{22}^*} + \frac{2K_{\mathrm{I}}K_{\mathrm{II}}}{D_{12}^*}\\ &\quad = \frac{B^2}{D_{11}^*}\left[\frac{a^3}{\pi R^2(1-\eta^2)^2}|I_1|^2 + \frac{\pi F^2}{a}|I_2|^2 - \frac{2aF}{R(1-\eta^2)}\,\mathrm{Im}\{\bar{I}_1 I_2\}\right],\end{aligned} \tag{50}$$

where we have used the identity

$$\frac{A^2}{D_{22}^*} + \frac{C^2}{D_{11}^*} - \frac{2AC}{D_{12}^*} = \frac{B^2}{D_{11}^*}. \tag{51}$$

Applying the Griffith criterion of energy balance

$$G = \tfrac{1}{4}\boldsymbol{K}^{\mathrm{T}}\boldsymbol{E}\boldsymbol{K} = \Delta\gamma, \tag{52}$$

where $\Delta\gamma$ is the work of adhesion, then yields a relation between the contact half width a and the pulling force F:

$$\begin{aligned}&\left(\frac{F}{\Delta\gamma}\right)^2 \frac{|g(\phi)|^2}{|\int_{-1}^{1}(1+\xi)^{-\bar{r}}(1-\xi)^{-r}\,\mathrm{d}\xi|^2}\\ &\quad - \frac{F}{\Delta\gamma}\left(\frac{a}{R}\right)^2 \frac{2R}{\pi(1-\eta^2)\Delta\gamma}\,\mathrm{Im}\left\{\bar{d}_1 g\,\frac{\int_{-1}^{1}(t(1+t)^r(1-t)^{\bar{r}}/(t-1))\,\mathrm{d}t}{\int_{-1}^{1}(1+\xi)^{-\bar{r}}(1-\xi)^{-r}\,\mathrm{d}\xi}\right\}\\ &\quad + \left(\frac{a}{R}\right)^4\left(\frac{R}{D_{11}^*\Delta\gamma}\right)^2 \frac{D_{11}^*}{\pi^2(1-\eta^2)^2 D_{22}^*}\left|\int_{-1}^{1}\frac{t(1+t)^{\bar{r}}(1-t)^r}{t-1}\,\mathrm{d}t\right|^2\\ &\quad - \frac{4a(D_{12}^{*2} - D_{11}^* D_{22}^*)\cosh^2 \pi\varepsilon}{\pi\Delta\gamma D_{12}^{*2} D_{22}^* B^2} = 0.\end{aligned} \tag{53}$$

Using the following relations:

$$\sqrt{\frac{D_{11}^*}{D_{22}^*} - \left(\frac{D_{11}^*}{D_{12}^*}\right)^2} = \frac{\sqrt{L_{11}L_{22}}}{L_{11}\cos^2\theta + L_{22}\sin^2\theta}, \quad \sqrt{\frac{1}{D_{11}^* D_{22}^*} - \frac{1}{D_{12}^{*2}}} = \sqrt{L_{11}L_{22}}, \tag{54}$$

$$\frac{D_{11}^*}{D_{22}^*} = \frac{\sin^2\theta + L_{22}\cos^2\theta/L_{11}}{\cos^2\theta + L_{22}\sin^2\theta/L_{11}}, \tag{55}$$

$$\frac{D_{11}^*}{D_{12}^*} = \frac{(L_{11}/L_{22} - 1)\,\sin\theta\,\cos\theta}{\cos^2\theta + L_{22}\sin^2\theta/L_{11}} \tag{56}$$

and

$$\frac{D_{11}^* D_{22}^*}{D_{12}^{*2}} = \frac{(L_{22}/L_{11} - 1)^2 \sin^2\theta\cos^2\theta}{(\cos^2\theta + L_{22}\sin^2\theta/L_{11})(\sin^2\theta + L_{22}\cos^2\theta/L_{11})}, \tag{57}$$

it can be shown that the normalized pulling force $F/\Delta\gamma$ depends on the normalized contact half width a/R via five parameters, L_{22}/L_{11}, $R/(D_{11}^{*}\Delta\gamma)$, η, θ and ϕ.

Numerical calculations will be used in the next section to analyze the influences of the material anisotropy orientation θ and the pulling angle ϕ on the critical force at pull-off, the critical contact half width and the adhesion strength.

4. Numerical analysis

Fig. 2 shows the normalized pulling force $F/\Delta\gamma$ as a function of the normalized contact half width a/R for different pulling angles ϕ under a set of chosen parameters $L_{22}/L_{11}, \eta, R/(D_{11}^{*}\Delta\gamma)$, and θ, and Fig. 3 shows the normalized pull-off force as a function

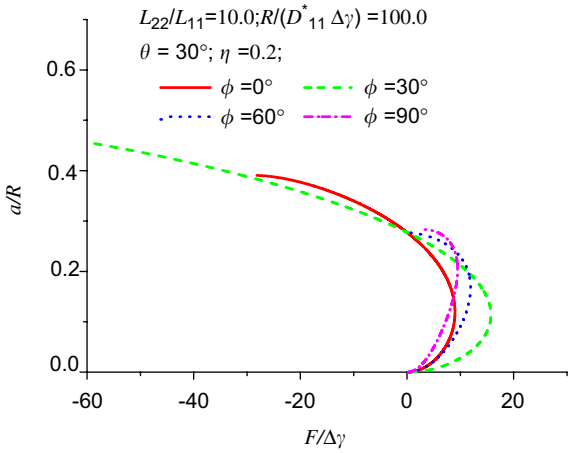

Fig. 2. The normalized contact half width a/R as a function of the normalized pulling force $F/\Delta\gamma$ for different pulling angles $\phi = 0, 30^{\circ}, 60^{\circ}, 90^{\circ}$ under a set of chosen parameters L_{22}/L_{11}, $R/(D_{11}^{*}\Delta\gamma)$, η and θ.

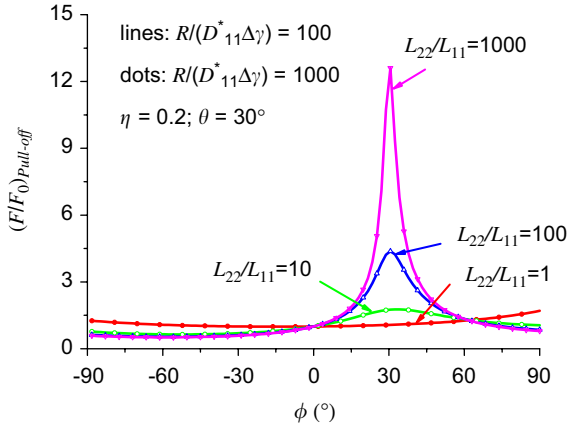

Fig. 3. The normalized pull-off force F/F_0 as a function of the pulling angle ϕ for $\eta = 0.2$, $\theta = 30^{\circ}$, $R/(D_{11}^{*}\Delta\gamma) = 100, 1000$ and different values of $L_{22}/L_{11} = 1, 10, 100, 1000$; F_0 denotes the pull-off force for $\phi = 0$. The solid lines are for $R/(D_{11}^{*}\Delta\gamma) = 100$ and the dots for $R/(D_{11}^{*}\Delta\gamma) = 1000$.

of the pulling angle ϕ. We find that the normalized pull-off force is almost independent of the parameter $R/(D_1^*\Delta\gamma)$. As a reference, the pull-off force for isotropic materials, corresponding to $L_{22}/L_{11}=1$, is shown to be relatively insensitive to the pulling angle ϕ. As the value of L_{22}/L_{11} increases, the material becomes increasingly anisotropic and the pull-off force shows increasing variation with the pulling angle ϕ, exhibiting a maximum value near $\phi=\theta$ (i.e., pulling along the stiff direction) and a minimum value at $\phi\approx\theta-\pi/2$ for $0\leqslant\theta\leqslant\pi/2$ or $\phi\approx\theta+\pi/2$ for $-\pi/2\leqslant\theta\leqslant 0$ (i.e., pulling along the soft direction). For L_{22}/L_{11} larger than 100, the maximum pull-off force can be an order of magnitude larger than the minimum pull-off force.

Fig. 4 shows the normalized critical contact half width at pull-off as a function of the pulling angle ϕ with the same parameters used in Fig. 3. One can see that the parameter

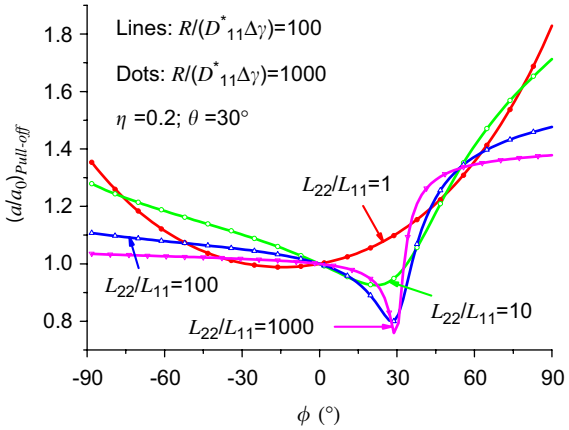

Fig. 4. The normalized critical contact half width a/a_0 at pull-off as a function of the pulling angle ϕ for $\eta=0.2$, $\theta=30^\circ$, $R/(D_{11}^*\Delta\gamma)=100,1000$ and different values of $L_{22}/L_{11}=1,10,100,1000$; a_0 denotes the critical contact half width for $\phi=0$. The solid lines are for $R/(D_{11}^*\Delta\gamma)=100$ and the dots for $R/(D_{11}^*\Delta\gamma)=1000$.

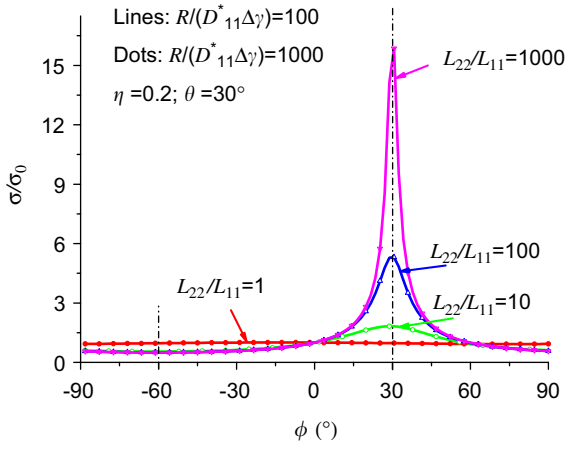

Fig. 5. The normalized adhesion strength σ/σ_0 as a function of the pulling angle ϕ for $\eta=0.2$, $\theta=30^\circ$, $R/(D_{11}^*\Delta\gamma)=100,1000$ and different values of $L_{22}/L_{11}=1,10,100,1000$; σ_0 denotes the adhesion strength for $\phi=0$. The solid lines are for $R/(D_{11}^*\Delta\gamma)=100$ and the dots for $R/(D_{11}^*\Delta\gamma)=1000$.

$R/(D_{11}^{*}\Delta\gamma)$ hardly affects the critical contact width. With increasing anisotropy (i.e., as L_{22}/L_{11} increases), the critical contact width exhibits a minimum value near $\phi=\theta$.

Another quantity that may be of interest is the adhesion strength which is defined as

$$\sigma=\frac{F_{\text{pull-off}}}{2a_{\text{pull-off}}}, \tag{58}$$

where $F_{\text{pull-off}}$ is the critical force and $2a_{\text{pull-off}}$ the critical contact width at pull-off. The normalized adhesion strength is shown as a function of the pulling angle ϕ in Fig. 5 with the same parameters used in Figs. 3 and 4. Again, while the adhesion strength does not vary significantly for different pulling angles in the isotropic case, it exhibits a distinct maximum at $\phi\approx\theta$ and a minimum at $\phi\approx\theta-\pi/2$ for $0\leqslant\theta\leqslant\pi/2$ or $\phi\approx\theta+\pi/2$ for $-\pi/2\leqslant\theta\leqslant0$ in the anisotropic cases. When the anisotropy ratio L_{22}/L_{11} exceeds 100, the maximum adhesion strength can be an order of magnitude larger than its minimum. The larger the L_{22}/L_{11}, the sharper the maximum peak.

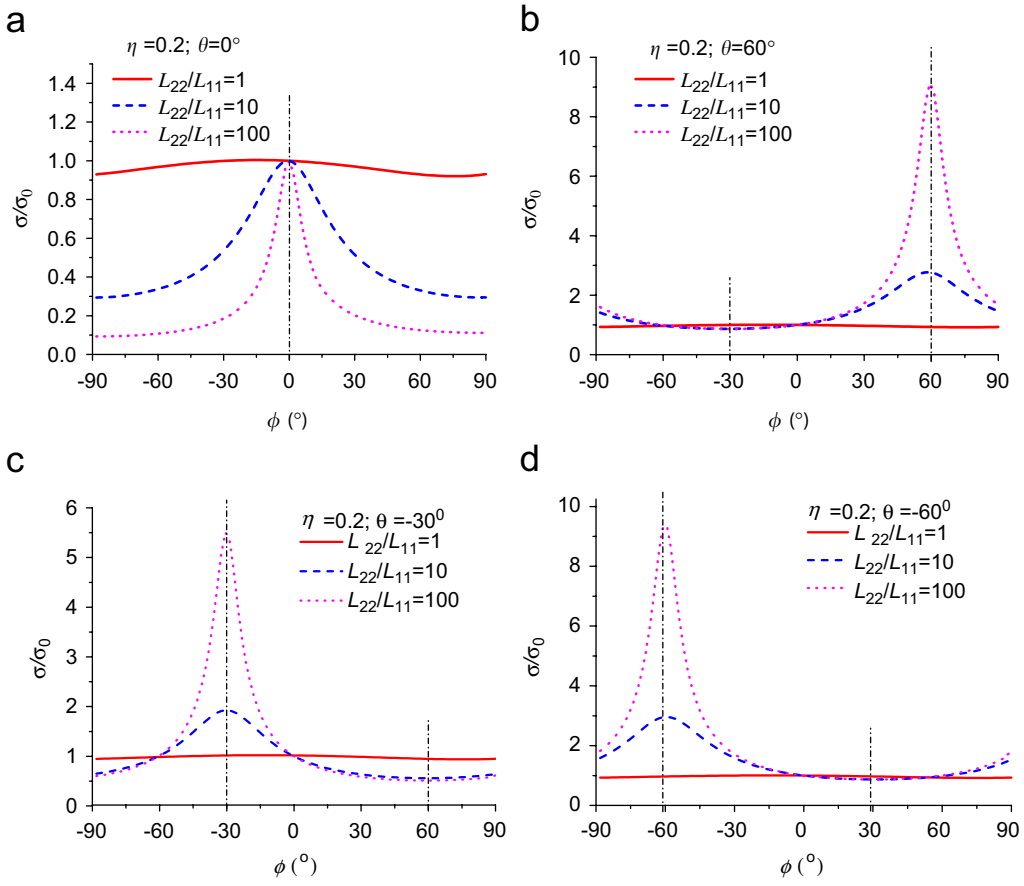

Fig. 6. The normalized adhesion strength σ/σ_0 as a function of the pulling angle ϕ for $\eta=0.2$ and $L_{22}/L_{11}=1,10,100$. (a) The case of $\theta=0^{\circ}$. (b) The case of $\theta=60^{\circ}$. (c) The case of $\theta=-30^{\circ}$. (d) The case of $\theta=-60^{\circ}$.

Similar behaviors of orientation-dependent adhesion strength have also been observed for other material orientations. A few examples are shown in Fig. 6 where the normalized adhesion strength is plotted as a function of the pulling angle ϕ for $\theta = 0^\circ$, 60°, -30° and -60°. These results all indicate that the adhesion strength exhibits a maximum when pulling in the stiff direction ($\phi = \theta$) and a minimum when pulling in the soft direction ($\phi = \theta - \pi/2$ for $0 \leqslant \theta \leqslant \pi/2$ and $\phi = \theta + \pi/2$ for $-\pi/2 \leqslant \theta \leqslant 0$). These results are fully consistent with, and confirmed from the contact mechanics point of view, the findings of Yao and Gao (2006) based on an interfacial fracture model between anisotropic elastic solids.

5. Summary and conclusions

The present paper has been aimed at developing a contact mechanics model for reversible adhesion in anisotropic elastic solids. In particular, the classical JKR model has been extended to adhesive contact between a rigid cylinder and a transversely isotropic elastic substrate. The analysis indicates that the adhesion force or strength exhibits a maximum value when pulling along the stiff direction and a minimum value when pulling along the soft direction of the transversely isotropic substrate material. For strongly anisotropic materials, the adhesion strength could vary more than an order of magnitude as the pulling angle changes. A switch between attachment and detachment can thus be accomplished simply by shifting the pulling angle. In contrast, the adhesion strength of an isotropic material is found to be relatively insensitive to the pulling direction. Such orientation-dependent adhesion provides a foundation for understanding reversible adhesion mechanisms in biological systems where adhesion must be not only robust but also easily reversible upon animal movement. Our analysis provides strong support, from the contact mechanics point of view, for the conclusion by Yao and Gao (2006) that strong elastic anisotropy leads to an orientation-controlled switch between attachment and detachment. The orientation-dependent adhesion induced by elastic anisotropy allows strong attachment in the stiff direction of the material to be released by shifting to pulling in the soft direction. This strategy has been summarized as "stiff-adhere and soft-release" (Yao and Gao, 2006).

The finding that elastic anisotropy leads to reversible adhesion provides a feasible explanation of why most biological adhesive tissues are anisotropic. The fibrillar adhesive tissue on geckos' feet is strongly anisotropic as the effective elastic modulus along the fiber direction is much higher than those normal to the fiber direction. The attachment pad of cicada shows a smooth top membrane covering an elongated foam structure which is expected to be strongly anisotropic. Similarly, the pad of the great green bush cricket (*Tettigonia viridissima*) is strongly anisotropic with a smooth membranous layer covering arrays of cross-linked rod-like fibers.

Acknowledgments

The work reported here was performed under the auspices of the Max Planck Society when H.G. served as a director at the Max Planck Institute for Metals Research in Stuttgart, Germany, in the last five years. S.C. gratefully acknowledges support by a Max Planck Visiting Scientist Fellowship during 2003 and 2005 and NSFC (10672165).

References

Arzt, E., Enders, S., Gorb, S., 2002. Towards a micromechanical understanding of biological surface devices. Z. Metallk. 93, 345–351.

Arzt, E., Gorb, S., Spolenak, R., 2003. From micro to nano contacts in biological attachment devices. Proc. Natl. Acad. Sci. USA 100, 10603–10606.

Autumn, K., Peattie, A.M., 2002. Mechanisms of adhesion in geckos. Integr. Comp. Biol. 42, 1081–1090.

Autumn, K., Liang, Y.C., Hsieh, S.T., Zesch, W., Chan, W.P., Kenny, T.W., Fearing, R., Full, R.J., 2000. Adhesion forces of a single gecko foot-hair. Nature 405, 681–685.

Autumn, K., Sitti, M., Liang, Y.C., Peattie, A.M., Hansen, W.R., Sponberg, S., Kenny, T.W., Fearing, R., Israelachvili, J.N., Full, R.J., 2002. Evidence for van der Waals adhesion in gecko setae. Proc. Natl. Acad. Sci. USA 99, 12252–12256.

Baney, J.M., Hui, C.Y., 1997. A cohesive zone model for the adhesion of cylinders. J. Adhes. Sci. Technol. 11, 393–406.

Barquins, M., 1988. Adherence and rolling kinetics of a rigid cylinder in contact with a natural rubber surface. J. Adhes. 26, 1–12.

Barthel, E., 1998. On the description of the adhesive contact of spheres with arbitrary interaction potentials. J. Colloid Interface Sci. 200, 7–18.

Beutel, R., Gorb, S., 2001. Ultrastructure of attachment specializations of hexapods (Arthropoda): evolutionary patterns inferred from a revised ordinal phylogeny. J. Zool. Syst. Evol. Res. 39, 177–207.

Carpick, R.W., Agrait, N., Ogletree, D.F., Salmeron, M., 1996. Variation of the interfacial shear strength and adhesion of a nanometer sized contact. Langmuir 12, 3334–3340.

Chaudhury, M.K., Weaver, T., Hui, C.Y., Kramer, E.J., 1996. Adhesion contact of cylindrical lens and a flat sheet. J. Appl. Phys. 80, 30–37.

Chen, S., Gao, H., 2006a. Non-slipping adhesive contact of an elastic cylinder on stretched substrates. Proc. R. Soc. London A 462, 211–228.

Chen, S., Gao, H., 2006b. Generalized Maugis–Dugdale model of an elastic cylinder in non-slipping adhesive contact with a stretched substrate. Int. J. Mater. Res. 97, 584–593.

Chen, S., Gao, H., 2006c. Non-slipping adhesive contact between mismatched elastic spheres: a model of adhesion mediated deformation sensor. J. Mech. Phys. Solids 54, 1548–1567.

Chen, S., Wang, T.C., 2006. General solution to two-dimensional nonslipping JKR model with a pulling force in an arbitrary direction. J. Colloid Interface Sci. 302, 363–369.

Derjaguin, B.V., Muller, V.M., Toporov, Y.P., 1975. Effect of contact deformations on the adhesion of particles. J. Colloid Interface Sci. 53, 314–326.

Dongye, C., Ting, T.C.T., 1989. Explicit expression of Barnett–Lothe tensors and their associated tensors for orthotropic materials. Q. Appl. Math. 47, 723–734.

Dundurs, J., 1969. Edge-bonded dissimilar orthogonal elastic wedges. J. Appl. Mech. 36, 650–652.

Gao, H., Yao, H., 2004. Shape insensitive optimal adhesion of nanoscale fibrillar structures. Proc. Natl. Acad. Sci. USA 101, 7851–7856.

Gao, H., Wang, X., Yao, H., Gorb, S., Arzt, E., 2005. Mechanics of hierarchical adhesion structures of gecko. Mech. Mater. 37, 275–285.

Glassmaker, N.J., Jagota, A., Hui, C.Y., Kim, J., 2004. Design of biomimetic fibrillar interface: 1. Making contact. J. R. Soc. Interface 1, 23–33.

Gorb, S., Beutel, R.G., 2001. Evolution of locomotory attachment pads of hexapods. Naturwissenschaften 88, 530–534.

Gorb, S., Scherge, M., 2000. Biological microtribology: anisotropy in frictional forces of orthopteran attachment pads reflects the ultrastructure of a highly deformable material. Proc. R. Soc. London B 267, 1239–1244.

Greenwood, J.A., 1997. Adhesion of elastic spheres. Proc. R. Soc. London A 453, 1277–1297.

Greenwood, J.A., Johnson, K.L., 1981. The mechanics of adhesion of viscoelastic solids. Philoon. Mag. 43, 697–711.

Greenwood, J.A., Johnson, K.L., 1998. An alternative to the Maugis model of adhesion between elastic spheres. J. Phys. D 31, 3279–3290.

Hiller, U., 1968. Untersuchunben zum Feinbau und zur Funktion der Haftborsten von Reptilien. Z. Morphol. Tiere 62, 307–362.

Huber, G., Gorb, S., Spolenak, R., Arzt, E., 2005. Resolving the nanoscale adhesion of individual gecko spatulae by atomic force microscopy. Biol. Lett. 1, 2–4.

Hui, C.Y., Glassmaker, N.J., Tang, T., Jagota, A., 2004. Design of biomimetic fibrillar interface: 2. Mechanics of enhanced adhesion. J. R. Soc. Interface 1, 35–48.

Hwu, C., 1993. Fracture parameters for the orthotropic bimaterial interface cracks. Eng. Fract. Mech. 45, 89–97.

Johnson, K.L., 1985. Contact Mechanics. Cambridge University Press, Cambridge.

Johnson, K.L., Greenwood, J.A., 1997. An adhesion map for the contact of elastic spheres. J. Colloid Interface Sci. 192, 326–333.

Johnson, K.L., Kendall, K., Roberts, A.D., 1971. Surface energy and the contact of elastic solids. Proc. R. Soc. London A 324, 301–313.

Kendall, K., 1975. The effects of shrinkage on interfacial cracking in a bonded laminate. J. Phys. D 8, 1722–1732.

Kesel, A.B., Martin, A., Seidl, T., 2003. Adhesion measurements on the attachment devices of the jumping spider *Evarcha arcuata*. J. Exp. Biol. 206, 2733–2738.

Kim, K.S., McMeeking, R.M., Johnson, K.L., 1998. Adhesion, slip cohesive zone and energy fluxes for elastic spheres in contact. J. Mech. Phys. Solids 46, 243–266.

Langer, M.G., Ruppersberg, J.P., Gorb, S., 2004. Adhesion forces measured at the level of a terminal plate of the fly's seta. Proc. R. Soc. London B 271, 2209–2215.

Maugis, D., 1992. Adhesion of spheres: the JKR-DMT transition using a Dugdale model. J. Colloid Interface Sci. 150, 243–269.

Morrow, C., Lovell, M., Ning, X., 2003. A JKR-DMT transition solution for adhesive rough surface contact. J. Phys. D 36, 534–540.

Muller, V.M., Yushenko, V.S., Derjaguin, B.V., 1980. On the influence of molecular forces on the deformation of an elastic sphere and its sticking to a rigid contact. J. Colloid Interface Sci. 77, 91–101.

Niederegger, S., Gorb, S., Jiao, Y., 2002. Contact behavior of tenent setae in attachment pads of the blowfly *Calliphota vivina* (Diptera, Calliphoridae). J. Comp. Physiol A 187, 961–970.

Robbe-Valloire, F., Barquins, M., 1998. Adhesive contact and kinetics of adherence between a rigid cylinder and an elastomeric solid. Int. J. Adhes. Adhes. 18, 29–34.

Roberts, A.D., Thomas, A.G., 1975. The adhesion and friction of smooth rubber surfaces. Wear 33, 45–64.

Russell, A.P., 2002. Integrative functional morphology of the *gekkotan* adhesion system (Reptilia: *Gekkota*). Integr. Comp. Biol. 42, 1154–1163.

Schwarz, U.D., 2003. A generalized analytical model for the elastic deformation of an adhesive contact between a sphere and a flat surface. J. Colloid Interface Sci. 261, 99–106.

Scherge, M., Gorb, S., 2001. Biological Micro- and Nano-Tribology—Nature's Solutions. Springer, Berlin.

Slifer, E.H., 1950. Vulnerable areas on the surface of the tarsus and pretarsus of the grasshopper (Acrididae, Orthoptera) with special reference to the arolium. Ann. Entomol. Soc. Am. 43, 173–188.

Spolenak, R., Gorb, S., Gao, H., Arzt, E., 2005. Effects of contact shape on the scaling of biological attachments. Proc. R. Soc. A 461, 305–319.

Ting, T.C.T., 1996. Anisotropic Elasticity. Oxford University Press, New York.

Wu, K.C., 1990. Stress intensity factors and energy release rate for interfacial cracks between dissimilar anisotropic materials. J. Appl. Mech. 57, 882–886.

Yao, H., Gao, H., 2006. Bio-inspired mechanics of robust and releasable adhesion on rough surface. J. Mech. Phys. Solids 54, 1120–1146.